Journal of Materials Chemistry

Cite this: J. Mater. Chem., 2012, 22, 12296

www.rsc.org/materials

PAPER

Vertical cobalt dendrite array films: electrochemical deposition and characterization, glucose oxidation and magnetic properties†

Jin You Zheng,‡[a] Zhen Lan Quan,‡[a] Guang Song,[a] Chang Woo Kim,[a] Hyun Gil Cha,[a] Tae Wan Kim,[a] Woonsup Shin,[a] Kyu Joon Lee,[b] Myung Hwa Jung[b] and Young Soo Kang*[a]

Received 16th January 2012, Accepted 23rd April 2012
DOI: 10.1039/c2jm30300k

Vertically and laterally oriented cobalt dendrite films with or without dendritic structures were synthesized by cathodic electrodeposition under different experimental conditions. The morphology of Co deposits was varied significantly depending on deposition conditions such as applied potential, precursor concentration and especially pH value. Co dendritic crystal growth along the [110] direction is preferred. The possible growth mechanism is discussed by supposing differing concentration areas. Results of glucose electrooxidation demonstrate that vertical Co dendrite films are promising materials as carbohydrate sensors with high sensitivity and fast response. In addition, magnetic measurements on cobalt samples under parallel and perpendicular direction of the applied magnetic field show that they exhibit a ferromagnetic behavior with different saturation magnetizations and coercivities.

1. Introduction

Metallic cobalt (Co) has attracted extensive attention as an important magnetic material not only due to its multiple crystal structures (hexagonal-close-packed (hcp), face-centered-cubic (fcc)) but also because of its structure dependent magnetic and electronic properties.[1] Elucidation of morphology-dependent properties of materials is essential for both fundamental understanding and technological application of materials.[2] Better understanding and control of material shapes will promote the design and production of optimal morphologies that can enhance the desired properties of materials. Various structures of metallic Co with different morphologies,[3] such as nanorods, nanowires, nanotubes, two- and three-dimensional (2D and 3D) superlattices, bowl-like and chain-like structures, have been successfully synthesized *via* different methods including thermal decomposition of organometallic precursors,[4] template-mediated synthesis,[5] electrospinning magnetic-field-induced process,[6] and hydro/solvothermal methods, *etc.*[7] Recently, dendritic materials have aroused wide interest in view of their importance in physics studies and their potential applications.[8] Cobalt dendrites are prepared commonly by hydro/solvothermal methods;[7a,9] however, these methods require high temperature and pressure, long time, or toxic chemicals such as hydrazine hydrate.

Dendritic fractals are one type of hyperbranched structure which are generally formed under non-equilibrium conditions.[10] It has been shown that dendritic fractals could be promising candidates for the design and fabrication of new catalytic functional nanomaterials[11] due to the distinct size, shape, and chemical functionality of such structures. The development of simple and novel synthetic approaches for building fractal architectures of various systems still remains as a challenge.

Unlike the conventional hydro/solvothermal synthesis, electrochemical deposition provides a route to prepare porous films or coatings rather than powders, which is of relevance to practical applications in fuel or solar cells, and sensors.[12] Especially, crystallization proceeds only *via* electrochemical reactions during electrodeposition, so that growth rate can be controlled by deposition potential or current, independently of the concentration of the reactants, different from supersaturation-based crystallization. Therefore, electrodeposition offers more freedom in creating various combinations of growth rate and diffusion rate, allowing for more systematic tailoring of the dendritic pattern.[13]

Most researches on dendrite materials have been focused on the synthesis methods, and there is a lack of research on the practical application of dendrite materials in different fields. Cobalt nanostructured materials are of considerable importance due to their special magnetic and catalytic properties. As an example, glucose detection is vital for the diagnosis and management of diabetes related diseases. It is also well known that glucose can provide an obvious potential source for biofuel cells[14] which is renewable, cheap and abundant. Enzymes have been widely used as catalysts in biofuel cells[15] and biosensors of glucose detection owing to their excellent chemical specificity.

[a]*Korea Center of Artificial Photosynthesis, Department of Chemistry, Sogang University, Seoul 121-742, South Korea. E-mail: yskang@sogang.ac.kr; Fax: +82-2-701-0967*
[b]*Department of Physics, Sogang University, Seoul, South Korea*

† Electronic supplementary information (ESI) available: Low magnification and cross-sectional SEM images, and XRD patterns. See DOI: 10.1039/c2jm30300k

‡ These authors contributed equally to the work.

About 40 years ago, Bursey *et al.*[16] had already prepared dendritic cobalt emitters by pulse electrodeposition. Imre *et al.*[17] also obtained centimeter-scale cobalt dendrites by an electrochemical method. Bodea and co-workers[18] utilized transmission electron microscopy to show cobalt arborescent growth in the electrodeposition process under the influence of an external magnetic field. Recently, Ri Qiu *et al.*[19] discussed time-dependent cobalt crystal morphology evolution; and later we also discussed on the various crystal growth parameters such as the potential, concentration and temperature, which affect the metallic cobalt crystal growth rate and the resultant morphology.[20] However, in previous works, few researchers prepared vertical cobalt dendrite array films with large area. In this work, a facile improved approach of preparing vertical dendritic Co films, which are composed of tens-of-micrometer-scale dendrites by electrochemical deposition is reported. The characterization of electrocatalytic and magnetic properties of the prepared Co films are also carried out.

2. Experimental

2.1 Electrodeposition

The electrodeposition of Co was performed in a conventional three-electrode cell using a potentiostat/galvanostat PL-9 instrument. Cu foil (Aldrich, ≥99.98%, 0.5 mm thickness) covered with Scotch tape on one side, which was polished by the emery paper on the side without tape and cleaned with deionized water and ethanol, was used as the working electrode. The area of Cu substrate dipped into 3 mL electrolyte solution was about 0.5 cm^2 (0.5 cm × 1 cm). A coiled platinum wire and Ag/AgCl electrode in 3 M KCl solution were used as counter and reference electrodes, respectively, and all potentials reported in this work were relative to the Ag/AgCl electrode. Co films were deposited from aqueous solutions containing 0.05 M $CoCl_2 \cdot 6H_2O$ (Sigma-Aldrich, 98%) and 0.1 M Na_2SO_4 (Ishisu Pharmaceutical, >99%) without stirring under ambient conditions at 24 °C. The applied potentials were in the range from −1.0 to −1.3 V. The pH of the solution was adjusted by adding 1 M NaOH solution (Junsei Chemical, Japan, >96%) or 0.5 M H_2SO_4 solution (Jin Chemical Pharmaceutical, Korea, >95%). After deposition for a given time, the electrode was removed and washed with deionized water and ethanol several times, and then dried at room temperature.

2.2 Characterization

X-Ray diffraction (XRD, Rigaku miniFlex-II desktop X-ray diffractometer, Cu-Kα radiation with $\lambda = 0.154056$ nm) was used to determine crystallinity and the crystal structure of the Co deposits. The morphologies of the samples were observed by a scanning electron microscope (SEM, Hitachi Horiba S-4300) operated at 20 kV and by a transmission electron microscope (TEM, JEOL. JEM-2010). Selected area electron diffraction (SAED, Oxford Instruments) patterns were measured to characterize the crystal structure of the deposits. For TEM and ED, the deposits were removed from the electrode by ultrasonication for 25 min. The elemental composition in the as-obtained materials was analyzed by energy dispersive spectroscopy (EDS, Oxford Instruments, INCA x-sight).

2.3 Electrochemical properties

The electrocatalytic properties of bare copper electrode and the copper electrodes modified by vertically and laterally oriented Co dendrites were tested by cyclic voltammetry (CV). The area of the electrode dipped into the solution was fixed to be 0.4 cm^2. Cyclic voltammetric measurements were carried out in a 10 mL aqueous solution of 0.1 M NaOH (Shinyo Pure Chemicals, G.R.) with and without 1.0 mM glucose (Katayama, First Class). The CVs were recorded in a potential range of −0.1 to 0.8 V *vs.* Ag/AgCl at a scan rate of 50 mV s^{-1}. The amperometric response towards glucose by the Co dendrite modified electrode was monitored by successive additions of glucose into 10 mL of 0.10 M NaOH solution with 1 mM changes in glucose concentration at 0.55 V *vs.* Ag/AgCl. All electrochemical experiments were conducted in a conventional three-electrode cell at room temperature, employing a coiled Pt wire electrode and an Ag/AgCl (3 M KCl) electrode as counter electrode and reference electrode, respectively.

2.4 Magnetic properties

A superconducting quantum interference device (SQUID) magnetometer was used to measure the magnetic properties of Co dendrites. The hysteresis loops were recorded at 300 K. The ZFC/FC curves were registered between 2 and 320 K at an applied magnetic field of 1000 Oe.

3. Results and discussion

3.1 Shape evolution of Co dendrite fractals

The typical electrodeposition of Co was carried out in an aqueous solution containing 0.05 M $CoCl_2$ and 0.1 M Na_2SO_4 with an initial pH of ~5.6 at different potentials. The solution system in this work is similar to that in Qiu's work.[19,20] Typical SEM images of the resulting Co deposits are shown in Fig. 1.

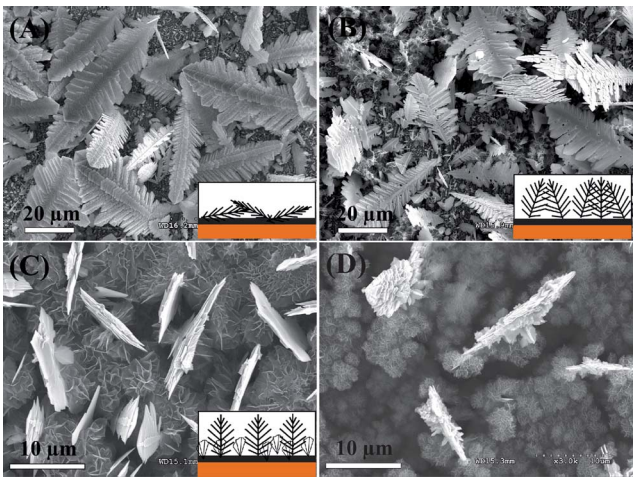

Fig. 1 SEM images of Co dendrite films deposited in 0.05 M Co^{2+} (precursor concentration: all solutions include 0.1 M Na_2SO_4) at pH 5.6 with different applied potentials for 600 s (deposition time). (A) −1.0 V, (B) −1.1 V, (C) −1.2 V and (D) −1.3 V (applied potential). Insets of (A), (B) and (C) are simplified schematic diagrams showing the morphologies of the as-obtained Co films.

There exist distinct differences in the morphology of Co deposits obtained at different potentials. With increasing potential the length of Co dendrites becomes shorter (from >50 μm (Fig. 1A) to <26 μm (Fig. S1B, ESI†)) and non-dendritic products (nanosheets) are increasingly formed. In our experiments, an increase in potential corresponds to a shift of applied potential to a negative direction. The applied potential of −1.0 V is more negative than the critical value for dendritic structure formation,[20] which is the reason that the dendrites can be formed. At −1.0 V, dendrites of >50 μm length are almost parallel to the surface of the Cu substrate. As the potential is increased from −1.1 to −1.3 V, the non-dendritic structures become more prominent while the dendrites are increasingly slanted or are vertical relative to the surface, as shown in Fig. 1B–D. Low magnification SEM images of Co films obtained at −1.2 and −1.3 V are shown in Fig. S1 (ESI†). At −1.3 V (Fig. 1D), the size of non-dendritic nanosheets becomes small and sub-dendrites grow on the surface of primary dendrites. To the best of our knowledge, it is difficult to make uniform micro-sized and flexible dendrites (metal, metal alloy and metal oxide) grow vertically on the substrate by electrodeposition. Here, we find that the Co dendrites can stand vertically with or without nanosheets in large area structures.

Fig. S2 (ESI†) shows XRD patterns of Co films obtained at different applied potentials from −1.0 to −1.3 V. All the peaks, except the peaks of Cu substrate, can be indexed to a pure hexagonal phase with space group of $P6_3/mmc$ (no. 194) of Co (JCPDS no. 05-0727). Co and $Co(OH)_2$ films composed of nanosheets have been reported.[21] To confirm the composition of products, EDS and EDS-mapping were employed for detailed analysis of the dendrites and nanosheets (as shown in Fig. 2). The atomic ratio of Co to O is about 95 : 5 in the dendritic structures while for the nanosheets, the atomic ratio of Co to O is *ca.* 66 : 21; S (8%) and Cl (4%) originate from the supporting electrolyte (Na_2SO_4 and $CoCl_2$). The trace amount of oxygen in the dendritic structure should be attributed to the partial oxidation of the external layer of cobalt products in the air. In the non-dendritic structure, the oxygen content is increased substantially, though most of this is from SO_4^{2-}. It is speculated that the non-dendritic structure is thus also metallic cobalt formed during electrodeposition at a relatively high potential. In addition, XRD patterns at different potentials (Fig. S2, ESI†) are similar for Co films with or without nanosheets also indicating that the nanosheets are also composed of metallic Co. At such a negative potentials, as-deposited Co is unlikely to be oxidized to form cobalt oxide or hydroxide.

The applied potentials can affect the deposition rate and determine the resulting morphologies of deposits;[8a,b,22] and we suspected that nanosheet Co films can be formed at a specific growth rate. The solution-based nature of electrochemical deposition allows for changing of many synthesis variables (*e.g.*, pH, additives, types of solvents and temperature) that markedly affect the growth direction and growth rates, and thus the final morphology of products.[23] To prove the assumption, the effect of Co deposition rate was investigated by varying the concentration of cobalt precursor, which would result in the change of deposition rate. Fig. 3 shows typical SEM images of Co deposits prepared in electrolyte with different cobalt precursor concentrations of 0.025 and 0.1 M at −1.1 V. With a high concentration of 0.1 M Co^{2+} (Fig. 3C and D), aggregated thicker dendrites without nanosheets were obtained, compared to the mixture formed in 0.05 M Co^{2+} at −1.1 V. In contrast, a large amount of Co nanosheets are formed at 0.025 M Co^{2+} (Fig. 3A and B) with only a few small dendrites being present. The Co^{2+} concentration has a dual role in the evolution of Co crystal morphology. On the one hand, the nucleation and growth rate of Co crystals could be accelerated with an increase in Co^{2+} concentration, leading to

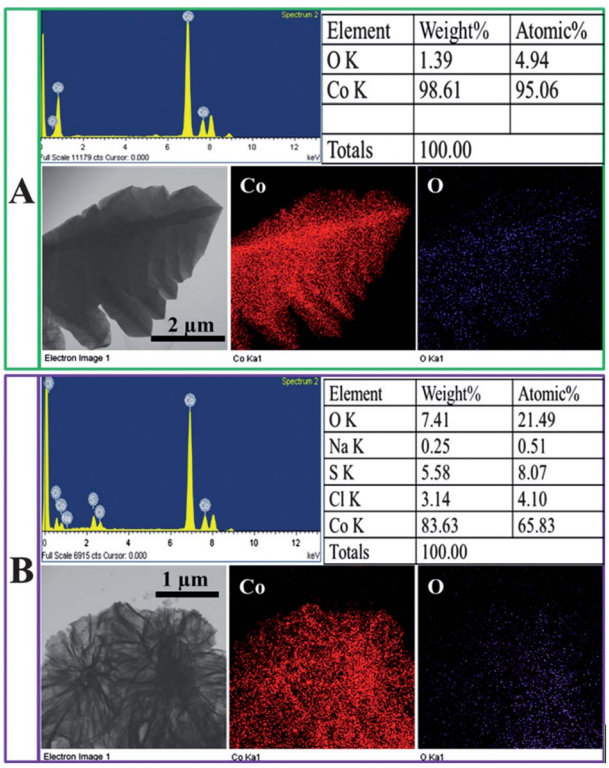

Fig. 2 EDS elemental analysis and EDS-mapping of (A) the dendrite and (B) the nanosheet Co deposits. Deposition condition: 0.05 M Co^{2+}, pH 5.6, −1.2 V, 600 s.

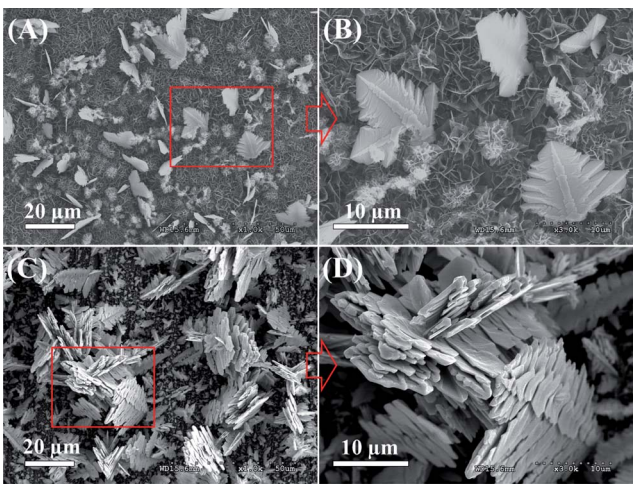

Fig. 3 SEM images of Co dendrite films obtained at different concentrations of Co^{2+}. Deposition conditions: pH 5.6, −1.1 V, 600 s; (A, B) 0.025 M, (C, D) 0.1 M.

local deficiency near the electrode surface because of faster consumption of Co^{2+}. On the other hand, it is easier to achieve mass diffusion controlled growth in a more dilute solution than in a concentrated solution with the same overpotential, due to a slower diffusion rate. As a result, the final morphology of Co deposits was determined by the balance between crystal growth rate and diffusion rate and the balance between concentration and potential, rather than solely by the concentration or potential.

To gain insight in the effect of pH on the crystal structure of final products, cobalt deposits were fabricated in the electrolyte at different pH and the morphology of the products was observed. Fig. 4 shows SEM images of Co deposits obtained at pH 7.5 with different potentials. At −1.1 V (Fig. 4A), the dendrites cling to the substrate (inset of A) and some nanosheet flowers adhere on the dendritic surfaces as shown in Fig. 4B. It shows clearly that the dendrites are composed of many hexagonal nanoplates. At −1.2 V (Fig. 4C and D), perfect Co dendrites of >60 μm length (Fig. S4A, ESI†) can stand vertically by clinging to each other (inset of C). It should be noted that single dendrites cannot stand vertically since the dendrite is flexible and the barycenter is too high and it is only possible for dendrites can grow vertically if they are not flexible, such as Pd nanotrees[24] (1 μm high and 100 nm thick). When the potential was increased to −1.3 V (Fig. 4E and F), a large amount of nanosheet flowers were formed and filled in the interspace of standing dendrites, which makes several dendrites cling to each other face to face and stand vertically (inset of E); the cross-sectional SEM image in Fig. S4B (ESI†) further corroborates this. As stated earlier, cobalt oxide or cobalt hydroxide are not readily obtained at relatively negative potentials or at the relatively high pH (7.5) as shown by the XRD patterns (Fig. S3, ESI†). The intensity of the (110) peak increases when the dendrites stand vertically. However, if the dendrites are covered with non-dendritic structures, the intensity of (110) peak is lowered and indicates that non-dendritic structures can affect the intensity of the (110) peak (Fig. S2, ESI†).

When pH was decreased to 2.5, as shown in Fig. 5, no cobalt nanosheets were formed. At a low potential of −1.1 V (Fig. 5A and B), only Co film composed of particles was obtained; this indicates that the growth rate is much lower than the mass-transport rate and no depletion area is formed.[22] At −1.2 V, a thermodynamically stable hexagonal morphology (Fig. 5C) was observed on some parts of the Co film and hexagonal plates without branches grew vertically. Polished metal electrodes have some scratched traces, which can be easily observed in Fig. 5A, C and E. A number of cobalt hierarchical structures[19] with 3 to 6 branches and with different sizes were formed as shown in

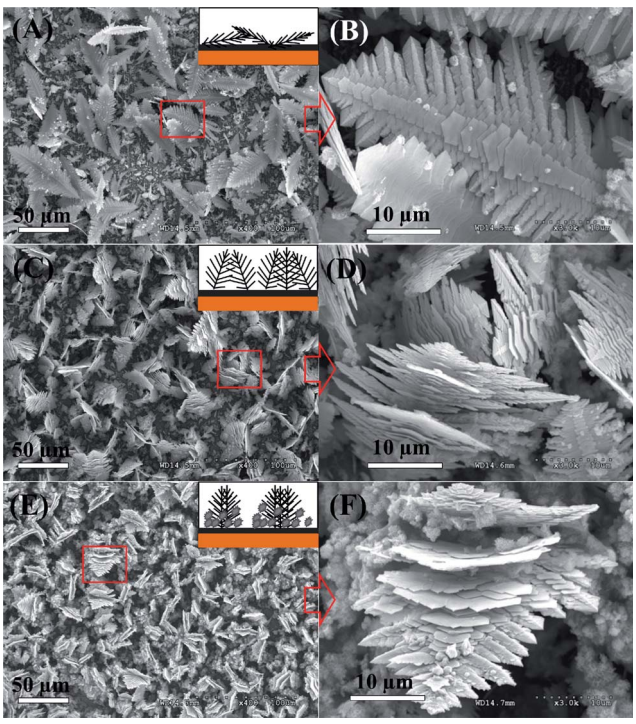

Fig. 4 SEM images of Co dendrite films deposited in 0.05 M Co^{2+} at pH 7.5 with different applied potentials for 600 s: (A, B) −1.1 V, (C, D) −1.2 V, (E, F) −1.3 V. Insets of (A), (C) and (E) are simplified schematic diagrams showing the morphologies of as-obtained Co films.

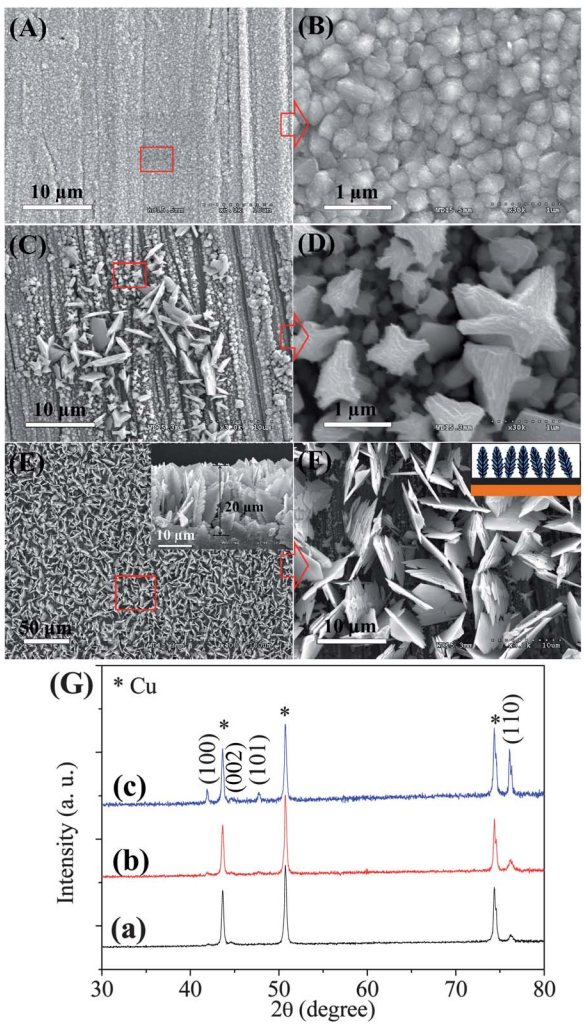

Fig. 5 (A–F) SEM images and (G) XRD patterns of Co films deposited in 0.05 M Co^{2+} at pH 2.5 with different applied potentials for 600 s: (A, B and a) −1.1 V, (C, D and b) −1.2 V, (E, F and c) −1.3 V. Insets of (E) and (F) are cross-sectional SEM images and the simplified schematic diagram of the as-obtained Co film, respectively.

Fig. 5D, and the majority of them showed asymmetrical growth. At a more negative potential of −1.3 V (Fig. 5E), vertical dendritic Co films with large area were obtained. All leaves were attached to the main stem in one side without forming any secondary branches and the other side is smooth. We denote this kind of inflexible dendrite as "semi-manufactured" since such dendrites appear to be intermediates for forming the normal dendritic structures such as the dendrites in Fig. 1A and B and Fig. 4.

Fig. 5G shows the XRD patterns of as-obtained Co films at pH 2.5 with potential from −1.1 to −1.3 V. The intensity of the (110) peak, rather than the (110) peak in JCPDS no. 05-0727, is maximum and indicates that Co crystal growth along the (110) direction is preferred in the electrodeposition process. In addition, the intensity of (110) increases as the density of vertical Co dendrites is increased. Comparing the XRD patterns in Fig. S2, S3 (ESI†) and Fig. 5G, it can be concluded that the intensity of the (110) peak becomes higher if there are more branches of Co dendrites and it is proposed that the Co dendrites grow parallel to the [110] plane.

To more clearly observe the evolution of crystal shapes and to delineate the crucial factors that determines the morphology of the final products, observations on the initial deposits fabricated with different deposition time were made. Fig. S5 (ESI†) shows SEM images of Co films obtained at pH 2.5 with the potential of −1.3 V for different deposition times. It was found that more crystals with larger size were formed for a longer deposition time. In the deposition process, the morphologies of Co change from grains to hexagons then to "semi-manufactured" dendrites with increasing deposition time. Fig. 6 shows typical TEM and SAED patterns of as-prepared samples. We examined SAED patterns of the leaves of the stems and branches of Co dendrites prepared in different conditions and at different growth stages of Co crystals. The results showed that the SAED patterns of the leaves in different areas of an individual dendrite are almost the same, which indicates that the leaves of Co dendrites grow along the (110) direction.

Co films obtained in Co^{2+} precursor aqueous solution with different deposition conditions show different features. When deposition was carried out in solution with relatively high pH (pH = 5.6 and 7.5), the crystal grew mainly by attachment of hexagonal plates to stems and finally formed Co dendrites while at low pH (pH = 2.5),"semi-manufactured dendrite" Co array films were formed. At low pH, the crystals showed a tendency to grow vertically instead of forming flat dendrites which are composed of hexagonal plates. The final morphology was produced during crystal growth. It is reasonable to conclude that the evolution from initial hexagonal nuclei to the morphology of final products goes through the crystal growth process at low pH such as pH = 2.5, and pH value of the electrolyte solution plays critical role to determine the final morphology. According to the experimental results in this work, it can be concluded that Co dendrites can grow laterally and vertically in the electrodeposition process with different deposition conditions, as shown in Scheme 1. A possible growth mechanism is shown in Scheme 1B. As we mentioned before, the final morphology of Co deposits was determined by the balance between crystal growth rate and diffusion rate and the balance between concentration and potential, and not simply by the magnitude of concentration or potential. To more readily understand the growth process of Co, it can be supposed that there are several concentration areas around the Co "*Crystal*" protrusion according to spherical diffusion layers around independently growing protrusions.[25] Here *Crystal* indicates products obtained at different stages of electrodeposition such as crystal seeds, particles or hexagonal plates. Normally, there will be a continuous concentration gradient around *Crystal*. Herein, we choose three concentration areas, C_1, C_2 and C_3, around *Crystal* to explain the results we obtained. The growth rate and direction at these three areas are represented by V_1, V_2 and V_3; and their directions are shown by the corresponding arrows. The brief explanations for different constructions as shown in Scheme 1A are explained as following.

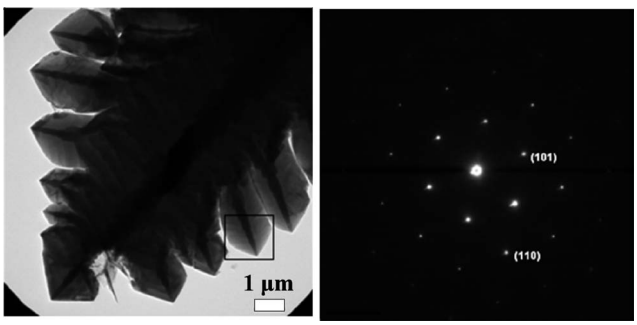

Fig. 6 TEM and SAED pattern of Co dendrites.

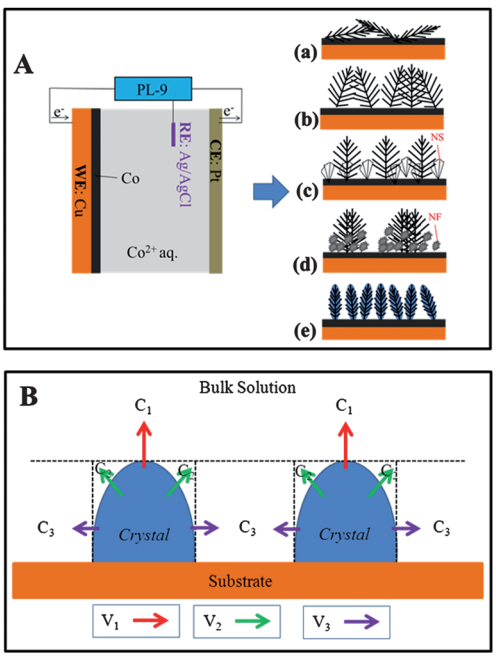

Scheme 1 (A) Simplified schematic diagram showing the different morphologies of as-obtained Co dendrite films by electrodeposition: (a) laterally oriented dendrites; (b) slanted dendrites clinging to each other; (c) dendrites standing vertically and separately with nanosheets (NS) between; (d) dendrites standing vertically clinging to each other face to face with nanoflowers (NF) between; (e) "semi-manufactured" dendrites standing separately with no non-dendritic structures. (B) Schematic diagram showing a possible growth mechanism.

(a) Laterally oriented dendrites on Cu substrate. At relatively low potential (but more negative than the critical value for dendrites) and near neutral pH (5.6, 7.5), the rates of electrocrystallization and mass-transfer are slow, so the density of Co crystal seeds is low. However, it is possible that the mass-transfer rate is faster than the crystallization rate so that C_3 is larger than both C_2 and C_3 (V_3 is thus the main growth direction) resulting under these conditions to lateral crystal growth due to an excess of Co^{2+} near the electrode surface.

(b) Dendrites are slanted by clinging to each other. If the potential is increased but not to so high a value, C_2 becomes bigger than C_1 and C_3. V_2 will be the main growth direction so that the dendrites can grow slanted relative to the surface.

(c) Dendrites stand up separately with nanosheets beneath. Crystals grow faster as the potential continuously increases. C_1 will be main growth direction; finally, vertically oriented dendrites formed on the substrate. In addition, non-dendritic structures (nanosheets) can be formed simultaneously given the very fast crystallization.

(d) Dendrites stand up vertically by clinging to each other face to face accompanied with nanoflowers. At relatively high pH (7.5) and high potential, the crystallization rate is so fast that vertical dendrites can grow from extraordinarily contiguous crystal seeds and the non-dendritic structures can be changed from nanosheets to nanoflowers.

(e) Inflexible separate vertical "semi-manufactured" dendrites with no non-dendritic structures. At high potential and low pH, the Co crystals grow only from V_1 direction. In this case, it also can be possibly attributed to the space hindrance effect (SHE) as for our previous report on a 1-D dendritic iron wire array.[26] The neighboring Co dendrites act as walls to block the mass transfer parallel to the substrate so that the crystals are enforced to grow along the perpendicular direction (V_1) by consuming the Co^{2+} precursor in the bulk solution. Study of the crystal growth mechanism of vertical Co dendrites is still underway in our laboratory.

3.2 Electrocatalytic and magnetic properties of Co dendrite films

Electrocatalytic activity, in order to explore application of the electrodeposited cobalt films as electrodes for glucose detection and glucose biofuel cells, in the electrooxidation of glucose on the cobalt modified electrodes was evaluated by cyclic voltammetry. Fig. 7 displays cyclic voltammograms of the Co dendrites with different morphologies in 0.1 M NaOH in the absence and presence of 1 mM glucose. Two typical electrodes A and B, which were modified with lateral and vertically oriented Co dendrites, were tested in the experiments. SEM images of the two electrodes comprising only dendritic structures are shown in Fig. 1A (inset of Fig. 7A) and 5E (inset of Fig. 7B). These electrodes were studied since dendritic Co films without Co nanosheets will show the exclusive properties of Co dendrites. Further, it is possible that Co nanosheets are readily oxidized or dissolved to form $Co(OH)_2$ or cobalt oxide in CV and amperometric response measurements.

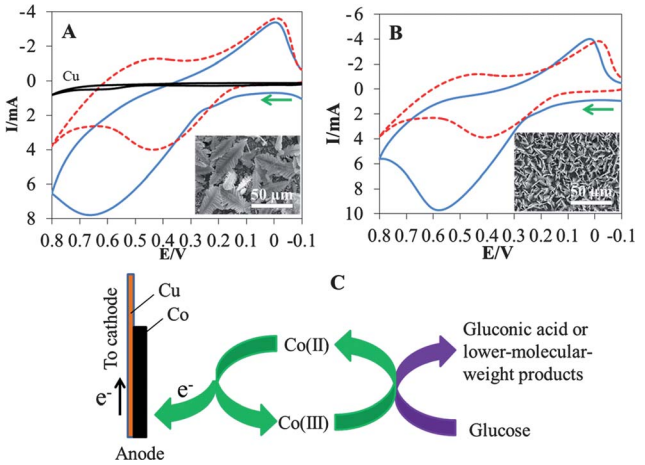

Fig. 7 CVs of bare Cu substrate (black solid line in A) in 0.1 M NaOH, (A) electrode A and (B) electrode B Co dendrite modified copper electrodes in 0.1 M NaOH without (red dashed line) and with (blue solid line) 1 mM glucose (scan rate: 50 mV s^{-1}; green arrows denote the scanning direction). (C) Schematic representation of the indirect electrooxidation of glucose by Co(II)/Co(III) redox couple present at the surface of Co films. Insets are SEM images of electrodes.

As indicated, both laterally and vertically oriented Co dendrite modified electrodes exhibited a pair of redox peaks in the absence of 1 mM glucose, which were related to the Co(II)/Co(III)[27] redox couple formed in alkaline medium. In contrast, with the addition of 1 mM glucose, notable enhancement of the anodic current could be observed. An obvious peak corresponding to glucose oxidation was detected in both cases, as shown in Fig. 7A and B. Glucose is catalytically oxidized with Co(III) species and this leads to C–C bond cleavage in alkaline solution to produce lower-molecular-weight products. An evident enhancement of the anodic current was observed, which demonstrates Co dendrite modified electrodes have high efficiency for glucose oxidation even in the micromolar scale. In addition, it is noteworthy that Co dendrites with different morphologies exhibited different electrochemical properties. When the electrode was modified with Co dendrites in a vertical direction (Fig. 7B), the potential of glucose oxidation was lower and the oxidation current was higher, compared to the Co dendrites in lateral direction (Fig. 7A). Such a substantial negative shift of the anodic peak potential, *i.e.* the decrease in the anodic overpotential, demonstrates stronger electrocatalytic performance in the glucose oxidation. The obvious increase in anodic current indicates that vertically oriented Co dendrite film has a higher sensitivity to glucose detection. Such a shift of oxidation potential can be attributed to a kinetic effect by an increase in the electroactive surface area and the rate of electron transfer from glucose to the Co modified electrode.[28] The electrode shown in Fig. 7B has a hierarchical structure, in which the open porous three-dimensional structure allows rapid transport of the solution, and its high surface area promotes electrochemical reactions. In order to clarify whether the copper substrate was involved in the electrocatalytic process or not, cyclic voltammetry behavior of copper substrate in NaOH solution containing 1 mM glucose was also monitored and the obtained curve was shown in Fig. 7A (curve Cu). The complete inactivity means it is

clear that Co dendrites deposited on the copper surface were responsible for the direct electro-oxidation of glucose.

Based on the electrocatalytic activity and cyclic voltammetric behavior, further experiments were carried out by employing the vertically oriented Co dendrite modified electrode B (as shown in Fig. 5E) at +0.55 V applied potential. Fig. 8A displays a typical amperometric response for the Co dendrite modified electrode to successive additions of glucose into 0.1 M NaOH at +0.55 V. It is observed that the electrode responds quickly to the change of glucose concentration and reaches a steady-state signal within 15 s without stirring. The amperometric signal showed a linear correlation to the glucose concentration, and the calibration curve for the glucose sensor is shown in Fig. 8B. The regression equation I (mA) = 0.1341 + 0.14365c (mM), with correlation coefficient of 0.9976 was obtained. The sensitivity of the Co dendrite modified electrode for glucose detection was 359.1 μA mM^{-1} cm^{-2}. The sensitivity of present electrode is higher than that of other nonenzymatic glucose sensors such as multi-walled carbon nanotubes (MWCNTs) array and Cu/MWCNTs or MnO_2/MWCNTs *etc.*[29] The results verify that Co dendrites, especially with vertically oriented 3D structures, are promising and potential materials for carbohydrate sensors and the properties of high sensitivity and fast response can be improved by controlling the morphology of products. The stability, selectivity, reproducibility and anti-interference property of the Co dendrite modified electrode requires further testing and optimization for possible application as a glucose sensor.

The magnetic behavior of Co dendrite films was investigated for vertically and laterally oriented Co dendrite modified electrodes B and A as shown in Fig. 9. Both show a ferromagnetic behavior at 300 K. The coercivities (H_c) of vertically oriented Co dendrite film (Fig. 9A) were about 140 and 50 Oe under perpendicular and parallel external magnetic fields, respectively. Similar results have been obtained previously for cobalt fibers and nanowires, and have been ascribed to the fact that the hexagonal c-axis is oriented close to the direction perpendicular to the fiber axis.[30] Magnetization of the vertical dendrite sample shows slower response under a perpendicular external magnetic field than under a parallel external magnetic field as shown in Fig. 9A. It is reasonable to deduce that the magnetic moments of the domains are oriented along the dendrite growth axis, resulting in an easy axis of magnetization along the long axis. In addition, the reason of a relatively low H_c value is due to the radial orientation of the dendritic branches which makes them difficult to be aligned simultaneously along the same direction.[31]

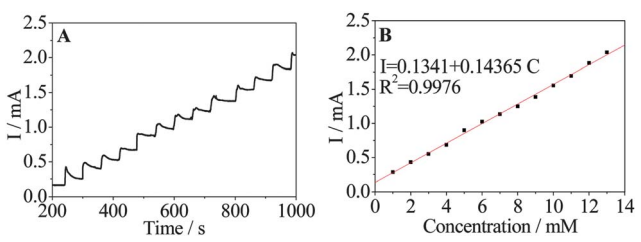

Fig. 8 (A) Amperometric response of vertically oriented Co dendrite modified copper electrode B (as shown in Fig. 5E) to subsequent additions of glucose in 1.0 mM steps in 0.1 M NaOH at +0.55 V. (B) The calibration curve of current *vs.* concentration of glucose.

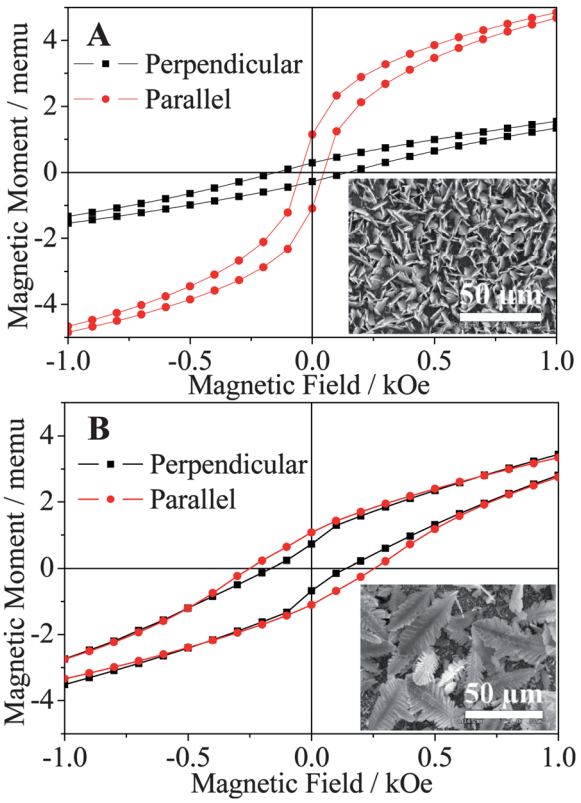

Fig. 9 Parallel and perpendicular hysteresis loops for (A) vertical electrode B (as shown in Fig. 5E) and (B) lateral electrode A (as shown in Fig. 1A) Co dendrite modified copper electrodes at 300 K. Insets are SEM images of electrodes.

For the laterally oriented dendrite film (Fig. 9B), H_c was about 140 and 250 Oe under perpendicular and parallel external magnetic fields, respectively. Magnetization responses under parallel and perpendicular external magnetic fields are very similar to each other (Fig. 9B). In contrast to the vertical Co dendrites, the coercivity under parallel external magnetic fields was larger than that under the perpendicular direction. This could be ascribed to the orientation of the hexagonal c-axis approximately parallel to the direction of Co dendrite growth.

The temperature-dependent magnetization of the Co-dendrite electrode A was measured in a range of temperature from 2 to 320 K under an applied magnetic field of 1000 Oe using zero-field-cooling (ZFC) and field-cooling (FC) procedures. Fig. 10 shows a typical result for Co dendrites with lateral growth. An irreversible magnetic behavior (difference between M_{FC} and M_{ZFC}) is evident in the whole range of temperature.[32] It can be found that the ZFC curve rapidly increases with temperature, and no clear blocking temperature (T_B), defined as the temperature with maximum magnetization in the ZFC curve, was observed. Co particles with size of lower than 20 nm have a distinct T_B as shown in some previous works.[33] Dakhlaoui *et al.*[30] reported similar results to ours, that submicrometric and micrometric Co fibers show no T_B (or a very low T_B response around 6 K arising from some small Co particles). However, the sizes of sub-branches and hexagonal Co plates in our sample are >1 μm as shown in TEM and SEM images, and even the particles on the bottom of dendrites are >100 nm as shown in Fig. S5A

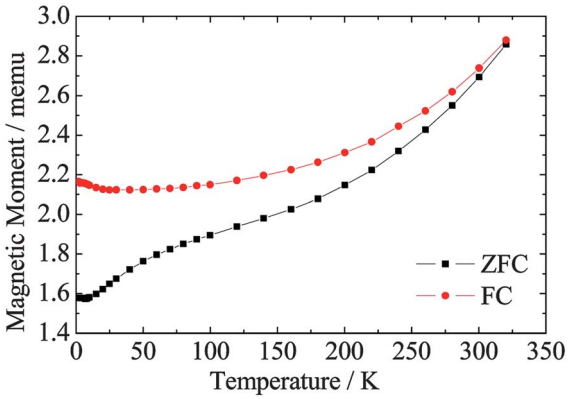

Fig. 10 ZFC and FC magnetization curves for lateral oriented Co dendrites at an applied external magnetic field of 1000 Oe.

(ESI†). These dimensions are not sufficiently small to create a mono-magnetic domain;[30] so leading to the non-observation of a blocking temperature in micro-sized dendritic Co. The continuous increase in the magnetization in the ZFC curve indicates a very wide energy-barrier distribution. The FC magnetizations showed a steady decrease with the decrease in the temperature, which is indicative of a strong dipolar magneto-static interaction between Co dendrites.

4. Conclusions

In summary, we have developed a facile approach of electro-chemical synthesis and tailoring of vertical Co dendrite fractals simply by controlling the deposition conditions. The morphology of Co deposits varied significantly depending on deposition conditions such as applied potential, precursor concentration and pH value. The possible growth mechanism is preliminarily discussed considering a model based on different concentration areas around growing crystals. Further work needs to be carried out for the better understanding of the mechanism of growth and in order to clarify the role of pH. The investigation in electro-catalytic activity of the dendritic Co films to glucose oxidation indicates the morphology and surface area dependence of the electrochemical behavior. Results demonstrate that vertical Co dendrite films could be promising materials for biofuel cells and as carbohydrate sensors with high sensitivity and fast response. Such properties can be optimized by controlling the deposition conditions. Magnetic measurements on cobalt samples under parallel and perpendicular direction of the applied magnetic field showed that they exhibit a ferromagnetic behavior with different saturation magnetization and coercivity in different directions, which may be attributed to their anisotropic shape. Irreversibility in the zero-field-cooling and field-cooling measurements was observed.

Acknowledgements

This work was supported by the Korea Center for Artificial Photosynthesis (KCAP) located in Sogang University funded by the Ministry of Education, Science, and Technology (MEST) through the National Research Foundation of Korea (NRF-2009-C1AAA001-2009-0093879).

Notes and references

1 V. F. Puntes, K. M. Krishnan and A. P. Alivisatos, *Science*, 2001, **291**, 2115.
2 (*a*) C. M. McShane and K. S. Choi, *J. Am. Chem. Soc.*, 2009, **131**, 2561; (*b*) Z. Zheng, B. Huang, Z. Wang, M. Guo, X. Qin, X. Zhang, P. Wang and Y. Dai, *J. Phys. Chem. C*, 2009, **113**, 14448.
3 (*a*) A. K. Srivastava, S. Madhavi, T. J. White and R. V. Ramanujan, *J. Mater. Chem.*, 2005, **15**, 4424; (*b*) Y. Zhu, Q. Yang, H. Zheng, W. Yu and Y. T. Qian, *Mater. Chem. Phys.*, 2005, **91**, 293; (*c*) Y. Hou, H. Kondoh and T. Ohta, *Chem. Mater.*, 2005, **17**, 3994.
4 (*a*) W. W. Ma, Y. Yang, C. T. Chong, A. Eggeman, S. N. Piramanayagam, T. J. Zhou, T. Song and J. P. Wang, *J. Appl. Phys.*, 2004, **95**, 6801; (*b*) F. Dumestre, B. Chaudret, C. Amiens, M. Fromen, J. Casanove, P. Renaud and P. Zurcher, *Angew. Chem., Int. Ed.*, 2002, **41**, 4286; (*c*) S. R. C. Vivekchand, G. Gundiah, A. Govindaraj and C. N. R. Rao, *Adv. Mater.*, 2004, **16**, 1842; (*d*) F. Dumestre, B. Chaudret, C. Amiens, M. Fromen, M. Respaud, P. Fejes, P. Renaud and P. Zurcher, *Angew. Chem., Int. Ed.*, 2003, **42**, 5213.
5 M. Knez, A. M. Bittner, F. Boes, C. Wege, H. Jeske, E. Mai and K. Kern, *Nano Lett.*, 2003, **3**, 1079.
6 (*a*) E. K. Athanassiou, P. Grossmann, R. N. Grass and W. Stark, *Nanotechnology*, 2007, **18**, 165606; (*b*) H. L. Niu, Q. W. Chen, H. F. Zhu, Y. S. Lin and X. Zhang, *J. Mater. Chem.*, 2003, **13**, 1803.
7 (*a*) L. P. Zhu, H. M. Xiao, W. D. Zhang, Y. Yang and S. Y. Fu, *Cryst. Growth Des.*, 2008, **8**, 1113; (*b*) L. Guo, F. Liang, X. Wen, S. Yang, L. He, W. Zheng, C. Chen and Q. Zhong, *Adv. Funct. Mater.*, 2007, **17**, 425; (*c*) Q. Xie, Z. Dai, W. W. Huang, J. B. Liang, C. L. Jiang and Y. T. Qian, *Nanotechnology*, 2005, **16**, 2958; (*d*) Q. Xie, Y. T. Qian, S. Zhang, S. Fu and W. Yu, *Eur. J. Inorg. Chem.*, 2006, 2454.
8 (*a*) R. Qiu, H. G. Cha, H. B. Noh, Y. B. Shim, X. L. Zhang, R. Qiao, D. Zhang, Y. I. Kim, U. Pal and Y. S. Kang, *J. Phys. Chem. C*, 2009, **113**, 15891; (*b*) R. Qiu, X. L. Zhang, R. Qiao, Y. Li, Y. I. Kim and Y. S. Kang, *Chem. Mater.*, 2007, **19**, 4174; (*c*) F. Tao, Z. Wang, D. Chen, L. Yao, W. Cai and X. Li, *Nanotechnology*, 2007, **18**, 295602; (*d*) J. Fang, H. You, P. Kong, Y. Yi, X. Song and B. Ding, *Cryst. Growth Des.*, 2007, **7**, 864; (*e*) J. Fang, X. Ma, H. Cai, X. Song and B. Ding, *Nanotechnology*, 2006, **17**, 5841; (*f*) Y. Yan, Q. S. Wu, L. Li and Y. P. Ding, *Cryst. Growth Des.*, 2006, **6**, 769.
9 (*a*) Y. Zhu, H. Zheng, Q. Yang, A. Pan, Z. Yang and Y. Qian, *J. Cryst. Growth*, 2004, **260**, 427; (*b*) X. Liu, R. Yi, Y. Wang, G. Qiu, N. Zhang and X. Li, *J. Phys. Chem. C*, 2007, **111**, 163; (*c*) X. M. Liu, W. L. Gao, S. B. Miao and B. M. Ji, *J. Phys. Chem. Solids*, 2008, 692665; (*d*) C. L. Jiang, L. Y. Wang and K. Kuwabara, *J. Solid State Chem.*, 2007, **180**, 3146; (*e*) G. X. Zhu, X. W. Wei, C. J. Xia and Y. Ye, *Carbon*, 2007, **45**, 1160–1166.
10 (*a*) T. A. Witten, Jr and L. M. Sander, *Phys. Rev. Lett.*, 1981, **47**, 351; (*b*) I. Lisiecki, P. A. Albouy and M. P. Pileni, *Adv. Mater.*, 2003, **15**, 712.
11 P. D. Yang, T. Deng, D. Y. Zhao, P. Y. Feng, D. Pine, B. F. Chmelka, G. M. Whitesides and G. D. Stucky, *Science*, 1998, **282**, 2244.
12 (*a*) M. J. Siegfried and K. S. Choi, *Adv. Mater.*, 2004, **16**, 1743; (*b*) M. J. Siegfried and K. S. Choi, *J. Am. Chem. Soc.*, 2006, **128**, 10356; (*c*) H. M. Kothari, E. A. Kulp, S. Boonsalee, M. P. Nikiforov, E. W. Bohannan, P. Poizot, S. Nakanishi and J. A. Switzer, *Chem. Mater.*, 2004, **16**, 4232; (*d*) E. A. Kulp and J. A. Switzer, *J. Am. Chem. Soc.*, 2007, **129**, 15120.
13 K. S. Choi, *Dalton Trans.*, 2008, 5432.
14 (*a*) A. Ramanavicius, A. Kausaite and A. Ramanaviciene, *Biosens. Bioelectron.*, 2005, **20**, 1962; (*b*) E. Katz, B. Filanovsky and I. Willner, *New J. Chem.*, 1999, **23**, 481; (*c*) N. Kakehi, T. Yamazaki, W. Tsugawa and K. Sode, *Biosens. Bioelectron.*, 2007, **22**, 2250.
15 F. Gao, Y. Yan, L. Su, L. Wang and L. Mao, *Electrochem. Commun.*, 2007, **9**, 989.
16 M. M. Bursey, C. E. Rochsteiner, M. C. Sammons, D. M. Hinton, T. S. Colpitts and K. M. Tvaronas, *J. Phys. E: Sci. Instrum.*, 1976, **9**, 145.
17 (*a*) A. R. Imre and L. Balázs, *Fractals*, 2000, **8**, 349; (*b*) A. Imre, Z. Vértesy, T. Pajkossy and L. Nyikos, *Fractals*, 1993, **1**, 59.
18 S. Bodea, R. Ballou, L. Pontonnier and P. Molho, *Phys. Rev. B: Condens. Matter*, 2002, **66**, 224104.

19 R. Qiu, P. Wang, D. Zhang and J. J. Wu, *Colloids Surf., A*, 2011, **377**, 144.
20 R. Qiu, D. Zhang, P. Wang, X. L. Zhang and Y. S. Kang, *Electrochim. Acta*, 2011, **58**, 699.
21 (*a*) H. Li and S. J. Liao, *J. Mater. Chem.*, 2009, **19**, 5207; (*b*) Y. G. Li and Y. Y. Wu, *Chem. Mater.*, 2010, **22**, 5537; (*c*) E. Hosono, S. Fujihara, I. Honma and H. S. Zhou, *J. Mater. Chem.*, 2005, **15**, 1938.
22 C. M. López and K. S. Choi, *Langmuir*, 2006, **22**, 10625.
23 K. S. Choi, *J. Phys. Chem. Lett.*, 2010, **1**, 2244.
24 F. Jia, K. Wong and L. Zhang, *J. Phys. Chem. C*, 2009, **113**, 7200.
25 K. I. Popov, B. N. Grgur, M. G. Pavlovic and V. Radmilovic, *J. Serb. Chem. Soc.*, 1993, **58**, 1055.
26 R. Qiu, J. Y. Zheng, H. G. Cha, M. H. Jung, K. J. Lee and Y. S. Kang, *Nanoscale*, 2012, **4**, 1565.
27 (*a*) E. Brillas and R. Sauleda, *J. Electrochem. Soc.*, 1998, **145**, 759; (*b*) P. N. Mashazi, K. I. Ozoemena and T. Nyokong, *Electrochim. Acta*, 2006, **52**, 177.
28 (*a*) Z. J. Zhuang, X. D. Su, H. Y. Yuan, Q. Sun, D. Xiao and M. M. F. Choi, *Analyst*, 2008, **133**, 126; (*b*) E. Reitz, W. Z. Jia, M. Gentile, Y. Wang and Y. Lei, *Electroanalysis*, 2008, **20**, 2482.
29 (*a*) X. H. Kang, Z. B. Mai, X. Y. Zou, P. X. Cai and J. Y. Mo, *Anal. Biochem.*, 2007, **363**, 143; (*b*) J. Chen, W. D. Zhang and J. S. Ye, *Electrochem. Commun.*, 2008, **10**, 1268.
30 A. Dakhlaoui, L. S. Smiri, G. Babadjian, F. Schoenstein, P. Molinie and N. Jouini, *J. Phys. Chem. C*, 2008, **112**, 14348.
31 L. P. Zhu, H. M. Xiao, W. D. Zhang, Y. Yang and S. Y. Fu, *Cryst. Growth Des.*, 2008, **8**, 1113.
32 D. Peddis, C. Cannas, A. Musinu and G. Piccaluga, *J. Phys. Chem. C*, 2008, **112**, 5141.
33 (*a*) C. Petit, A. Taleb and M. Pileni, *Adv. Mater.*, 1998, **10**, 259; (*b*) G. H. Wen, R. K. Zheng, K. K. Fung and X. X. Zhang, *J. Magn. Magn. Mater.*, 2004, **270**, 407.

